Study of low-frequency quasi-periodic oscillations in GRS 1739-278 during 2014 outburst

Authors[1]

[1]*Space Research Institute, Russian Academy of Sciences, Profsoyuznaya 84/32, 117997 Moscow, Russia*

ABSTRACT

We detected low-frequency quasi-periodic oscillations (QPOs) at 0.3..2 Hz in *NuSTAR* and *Swift-XRT* observations of black hole candidate GRS 1739-278 during its 2014 outburst.

1 INTRODUCTION

A study of X-ray variability in accreting astrophysical sources provides a broad view on processes that take a place in such systems. This works both on a long timescales - i.e. days and weeks - when one speak about state changes through outbursts of transients sources (see e.g. Homan and Belloni 2005a; Heil et al. 2015), and on short - all the way down to milliseconds - when the subject under consideration are a quasi-periodic oscillations (QPOs). By simultaneous usage of spectral and timing data one can better constrain geometry of accretion flow around compact objects and infer on which processes are responsible for generation of observed spectro-timing features in a self-consistent way.

Some aspects of the spectro-timing evolution of the X-ray transients (usually black-hole candidates, BHC) during outbursts can be explained in the frame of the two-temperature accretion flow model (Eardley et al. 1975; Shapiro et al. 1976; Narayan and Yi 1995), in which geometry of system consists of the geometrically thin cold disk and geometrically thick hot flow (corona), which is thought to be responsible for production of strong variability. As example, using frequency-resolved spectroscopy Churazov et al. (2001) shown that variable part of the emission has a hard spectrum, produced by Comptonization of soft photons onto hot electrons in the corona, while stable part of the emission has a spectrum which is consistent with the cold classical α-disc spectrum (Shakura and Sunyaev 1973). Lyubarskii (1997) proposed that observed strong variability (seen as a broad band noise in power spectra) is produced due to the stochastic variations of the angular momentum transport efficiency. In this propagating fluctuation model broad band noise is a product of noise signals from different radii of the accretion flow, each with its own characteristic time-scale (see, e.g. Arévalo and Uttley 2006; Ingram and van der Klis 2013). Therefore, the shape of the broad band noise is determined by the physical and geometrical properties of the accretion flow, e.g. in particular in these works it was suggested that the broad noise dumping frequency is connected to the inner edge of the accretion flow.

Another feature, frequently observed in the X-ray binaries power spectra is different types of low and high frequency QPOs, manifesting itself as a narrow Lorentzian components. One of the long-standing questions in X-ray timing is the origin of so called type-C low-frequency QPOs (see Casella et al. 2005, for LFQPO classification), which are often found in X-ray binaries harboring both neutron stars and black-holes (Wijnands and van der Klis 1999a) during initial rise and transition to disk dominated state (in low-hard state (LHS) and in hard intermediate state (HIMS)), according to standard scheme (Grebenev et al. 1997; Tanaka and Shibazaki 1996; Remillard and McClintock 2006; Belloni 2010)). This QPOs are widespread and easy to detect and study, since they occur at moderate frequencies of 0.1..10 Hz and prominent, having $rms \approx 10\%$. Different author prescribe generation of this QPOs to various processes: Lense-Thirring precession of inner parts of accretion disk (Stella and Vietri 1998a; Ingram et al. 2009a), oscillations of standing shock (Molteni et al. 1996), accretion rate modulation caused by different phenomena (Tagger and Pellat 1999; Cabanac et al. 2010) e.t.c. In some models, particularly in relativistic precession models (RPM), observed frequency is strongly dependent on location of inner part of cold accretion disk.

Recent advances in simulating the reflection (Ross and Fabian 2005; **García** et al. 2014), arising from reproduction of emission from central engine by accretion disk, led to the possibility to study geometry of accretion disk in bright systems. For such a study to be made it is essential to obtain broadband X-ray spectrum with high energy resolution - reflected component manifest itself by a presence of prominent, wide and asymmetric iron K_α-line at 6.4 keV and Compton-hump at 20-30 keV. Now, adding information from X-ray timing one can, in principle, constrain the location of a component, responsible for the variability - which is though to be corona or jet foundation. This task present a challenge, that can be solved only by a telescope

that posses both possibility to measure broadband spectrum with good resolution and have a corresponding timing capabilities. *NuSTAR* (Harrison et al. 2013), launched in 2013, is the best available instrument for such studies, although, except for observations in energy band above 12 keV, *XMM-Newton* (and *NICER* in the nearest future) can be used too, producing some great results (Ingram et al. 2016).

In this article we report on first detection of this QPOs in HIMS of Galactic black-hole candidate GRS 1739-278 and present a detailed study of properties of the X-ray variability, along with spectral evolution.

2   GRS 1739-278

GRS 1739-278 is a typical X-ray nova, discovered during outburst in 1996 (Paul et al. 1996) by *SIGMA* (Paul et al. 1991) telescope onboard *GRANAT* space observatory. Using *ROSAT* observation Greiner et al. (1996) inferred distance of 6–8.5 kpc, indicating that source may belong to Galactic bulge. Optical and radio emission were detected during the course of outburst (Hjellming et al. 1996; Marti et al. 1997). Borozdin et al. (1998) found spectral evolution throughout outburst to be consistent with canonical model - outburst starts from LHC, then soft component, associated with disk emission starts to dominate, heralding transition to high-soft state. Eventually, they observed very high state and detected a QPO at 5 Hz using *RXTE* data (Borozdin and Trudolyubov 2000).

After some 18 year slumber GRS 1739-278 demonstrated another big outburst, rise of which was detected by *Swift-BAT* (Krimm et al. 2014) along with *INTE-GRAL* (Filippova et al. 2014). During this outburst extensive observing campaign by *Swift-XRT* were carried out, along with single long *NuSTAR* exposure. We will utilize this data in following chapters. After this outburst source remain active with repetitive mini-outbursts (Mereminskiy et al. 2016; Yan and Yu 2017).

3   OBSERVATIONS AND DATA REDUCTION

In order to characterize the overall outburst profile we used data of *Swift-BAT transient monitor* (Krimm et al. 2013) in hard X-rays (15–50 keV) as well as data from *MAXI* (Matsuoka et al. 2009) (2–4 keV).

We used public observations of *Swift-XRT* (target ID: 33203) performed regular over the peak and decline of the outburst. Since the source was bright, all *Swift-XRT* observations were performed in windowed mode, allowing study of timing properties of the source. We performed standard analysis with `xrtpipeline` and barycentered data prior to lightcurve extraction. During several observations countrate was as high as 280 cts s^{-1}, therefore we excluded one or few brightest columns, in order to suppress effects caused by photon pile-up. Long-term lightcurves and spectra were obtained from UK Swift Science Data Centre at the University of Leicester (Evans et al. 2009).

We also used *NuSTAR* observation (ObsID: 80002018002) performed at March 26, 2014 (MJD 56742). `nuproducts` pipeline were utilized to extract photons from two-arcminute circular region, centered on source and to produce lightcurves and spectra.

4   ANALYSIS

4.1   Outburst

First detection of the source by *Swift-BAT* (Krimm et al. 2014) occurred at March 9, 2014 (MJD 56725, we will refer to this date as τ_0). Outburst profile in hard X-rays (15–50 keV) featured fast rise with tenfold intensity increase over ten days, nearly flat-top peak ($\tau_0+10..+15$) followed by abrupt flux decrease by 30% over two days. After this, source demonstrated gradual decline interrupted by flaring activity at $\tau_0+30..+65$. Another interesting feature is dip, observed in *Swift-BAT* lightcurve at $\tau_0 \approx +86$. After the cease of the outburst source remained active with flux about 5–15 mCrab.

Adding softer data from *MAXI* to the *Swift-BAT* hard X-ray lightcurve gives us another insight on evolution of the outburst as shown in Fig. 1 - comparing fluxes in soft and hard bands (for 2–4 keV band we took a 1.67 counts s^{-1} as a reference value for Crab, corresponding value for 15–50 keV band is 0.22 cts cm^{-2} s^{-1}) one can see that soft component obviously lags hard emission in the beginning of the outburst but then start to grow and ends up dominating during the flaring period as well as hard dip(s). Lower subplot of Fig. 1 shows evolution of hardness ratio (3–10 keV/0.8–3 keV) measured by *Swift-XRT*. Right after peak of hard X-rays one can see decline of hardness, also indicating appearance of thermal component.

Fortunately, the *NuSTAR* observation triggered by Miller et al. (2015) were carried right at the transition between hard and soft states, thus giving us unique possibility to study processes that happens during HIMS.

4.2   NuSTAR observation

NuSTAR observed GRS 1739-278 (ObsID: 80002018002) for nearly 30 ks of dead-time corrected exposure right after hard X-ray peak (see Fig. 1). Earlier, Miller et al. (2015) shown that the average spectrum of this observation is well described by reflection models such as *relxill* (**García** et al. 2014; Dauser et al. 2014, 2016) with accretion disk that reaches remarkably close to the black hole innermost stable circular orbit (ISCO), with upper estimate being $r_{in} = 5^{+3}_{-4} \, GM/c^2$ (Miller et al. 2015). Interestingly, no additional thermal component was needed in order to obtain a good fit, probably because of *NuSTAR* energy band, starting at 3 keV.

Given the 96.9 minute orbital period of *NuSTAR*, observation is divided in 13 intervals separated by Earth occultations, as shown in Fig. 2. We denoted this intervals with roman numerals, from **I** to **XIII**. From the lightcurve of observation it is clear, that source flux is increasing throughout observation from $\approx$145 counts per second up to $\approx$170 counts per second. The spectrum also alter, with hardness (defined as ratio of countrates $R_{3-10\,keV}/R_{10-78\,keV}$) monotonically growing from 2.5 to 3.5.
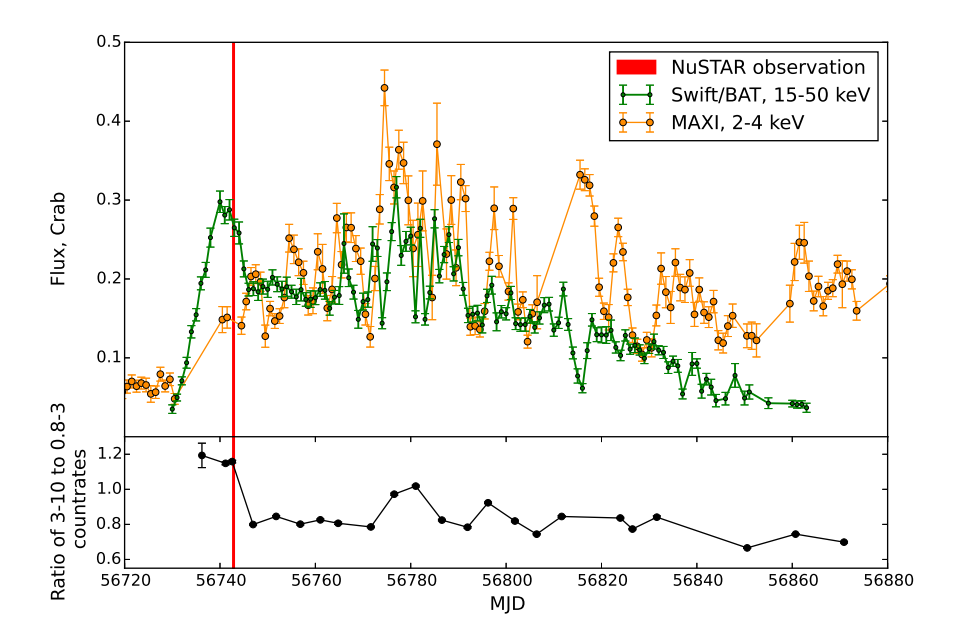
Figure 1. *Upper:* green points denote *Swift-BAT* lightcurve of second outburst in 15–50 keV range, orange circles correspond to *MAXI* fluxes in 2–4 keV. Red line show time of *NuSTAR* observation. *Lower:* evolution of *Swift-XRT* spectral hardness during the outburst.

4.2.1 Continuum evolution

To get better view on evolution of continuum emission we fitted using `XSPEC` package (Arnaud 1996) all individual interval spectra with `xillver` model (García et al. 2013). This model describes reflection of incident radiation from ionized slab of matter. The spectrum of incident radiation are assumed to be power-law with exponential cutoff. Spectra from two *NuSTAR* modules of each interval were fitted simultaneously with `phabs*const*xillver` model. We choose to fix interstellar absorption at $N_H = 2.15 \times 10^{22}$ cm^{-2} as was found by joint *XMM-Newton/NuSTAR* observation during low luminosity state (Fuerst et al. 2016). Element abundances were taken from Wilms et al. (2000) and cross-sections from Verner et al. (1996). Relative iron abundance were fixed at $A_{Fe} = 1$, ionization parameter at $\xi = 3.2$ and inclination at 35 degrees. This parameters are in agreement with measured by Miller et al. (2015) with different spectral models. Although in `xillver` there is no relativistic broadening of Fe-line no significant residuals in 5–8 keV region are seen, mainly because of limited statistics in per interval spectra. Before fitting, spectra were grouped in order to have at least 100 counts per bin, channels above 60 keV were ignored. Resulting fits are of satisfactory quality with mean $\chi^2_{red.} \approx 1.05$.

Examination of best-fit parameters shown in Fig.4 confirms that spectrum softens during observation and cutoff energy decreases. Flux is steadily increasing and at the end of observation unabsorbed luminosity in 3–60 keV band reach 7×10^{37} erg s^{-1} assuming 8 kpc distance.

4.2.2 Constrains on movement of the inner parts of accretion disk

Yet, spectra of single intervals have not enough statistics to constrain change of Fe-line profile and, hence, to determine

is the inner boundary of disk is moving during observation. To increase statistics, we split whole observation into three major pieces, with first made by intervals **I-IV**, second by **V-IX** and third by **X-XIII** and extracted 4–78 keV spectra. We chose to group them in order to have at least 100 counts per bin and then we fitted them (excluding data between 5–10 keV) with simple `phabs*cutoffpl` model, using, once again, $N_H = 2.15 \times 10^{22}$ cm^{-2}.

Now, plotting the ratio of this fit to initial spectra (see Fig. 3) one can see that both strong features - i.e. Fe-line complex at 5–9 keV and Compton hump around 30 keV are seemingly stable. Therefore we can conclude, that there is no drastic change in position of inner disk boundary between parts of observation. Additionally, we estimated equivalent width of Fe-line in this three parts - we approximated 4–78 keV spectra with 10–30 keV range being ignored (to neglect the Compton-hump contribution) with model consisting of absorbed cut-off powerlaw and gaussian. Equivalent width of gaussian component remain constant within error margins, around 0.175 keV, although it is possible that the quality of data is not enough to trace real change.

4.2.3 Characterization of the average spectrum

There is a 1.3 ks part of *Swift-XRT* snapshot (ObsId: 00033203003) that coincides with *NuSTAR* observation. Extension of an energy range to 0.8 to 78 keV allow one to search for thermal emission associated with cold inner disk with $kT \sim 0.1...0.4 keV$ (such as were found in other BHCs, see (Miller et al. 2006a,b; Parker et al. 2015, e.t.c)).

We extracted *Swift-XRT* spectrum using only zero-grade events, and grouped it (as well as *NuSTAR* spectra) to have 30 counts per bin. We used latest available version of *relxilllp* package (v1.0.2), the model that describes reflection of emission, produced by point source located on the rotation axis above the Kerr black hole, from the relativistic
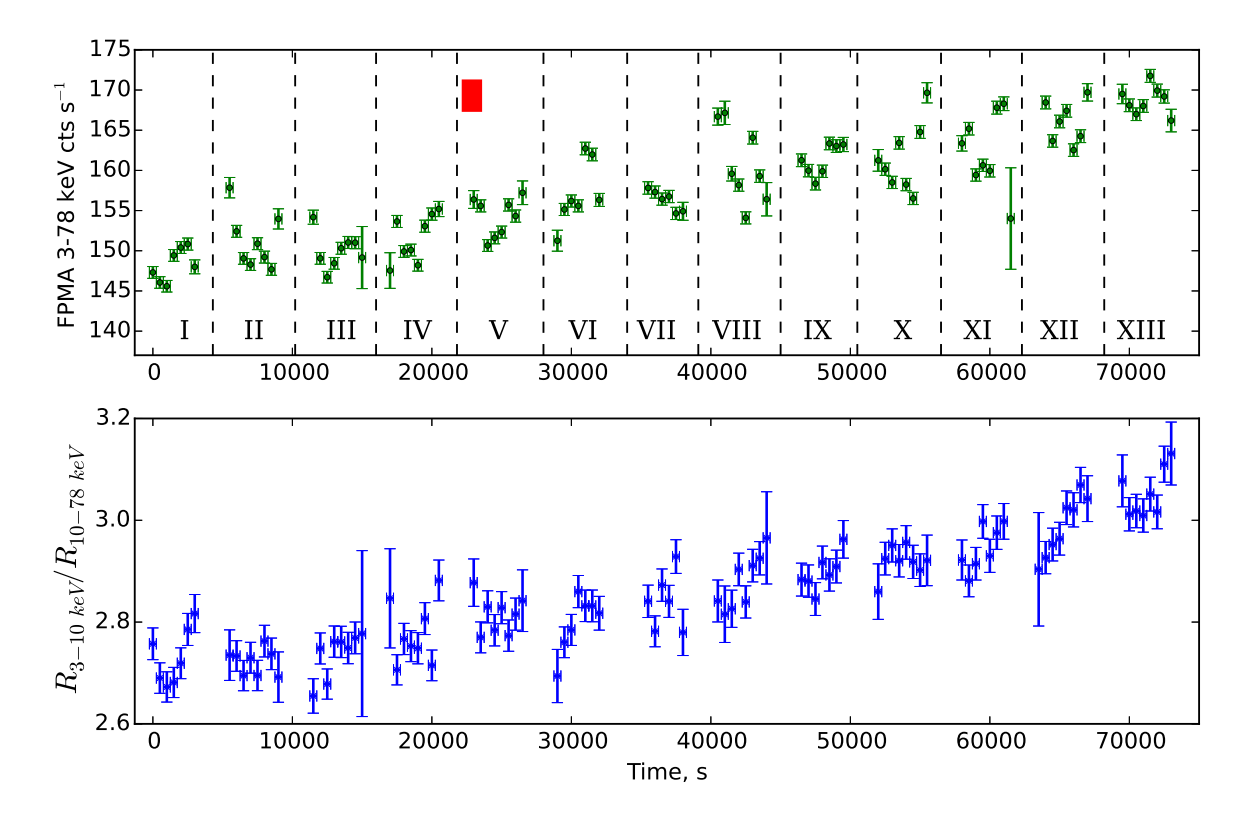
Figure 2. Upper panel: countrate of *NuSTAR* FPMA in 3–78 keV band. We enumerated intervals of uninterrupted observations with roman numerals. Red square shows time of simultaneous *Swift-XRT* observation (ObsId: 00033203003, second part). Bottom panel: evolution of hardness during observation
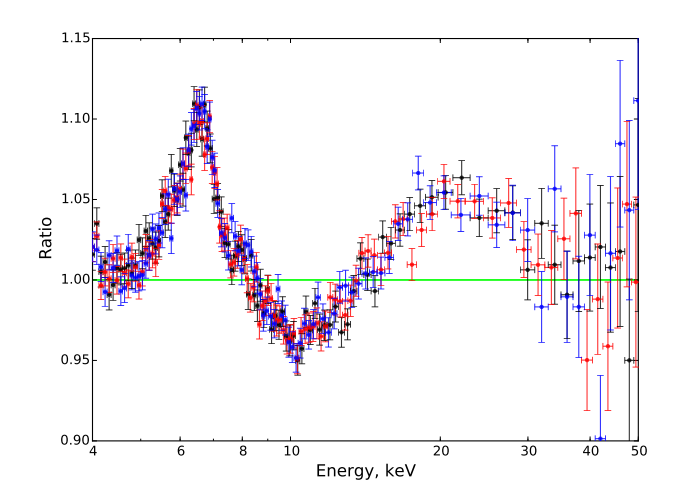

Figure 3. Ratio of *NuSTAR* FMPA, spectra to `phabs*cutoffpl` model. In black - data from intervals I-IV, in red from V-IX and in blue from X-XIII.

accretion disk. Among the parameters of model several of particular interest - namely $\Gamma_1, \Gamma_2, R_{br}$ - i.e parameters that describe emissivity profile along radius and, of course, R_{in}, location of the inner boundary of accretion disk. This model was selected for several reasons - first, Miller et al. (2015) found that it match observed data well, second, during the 1996 outburst source were detected at radiowaves, possibly indicating jet activity.
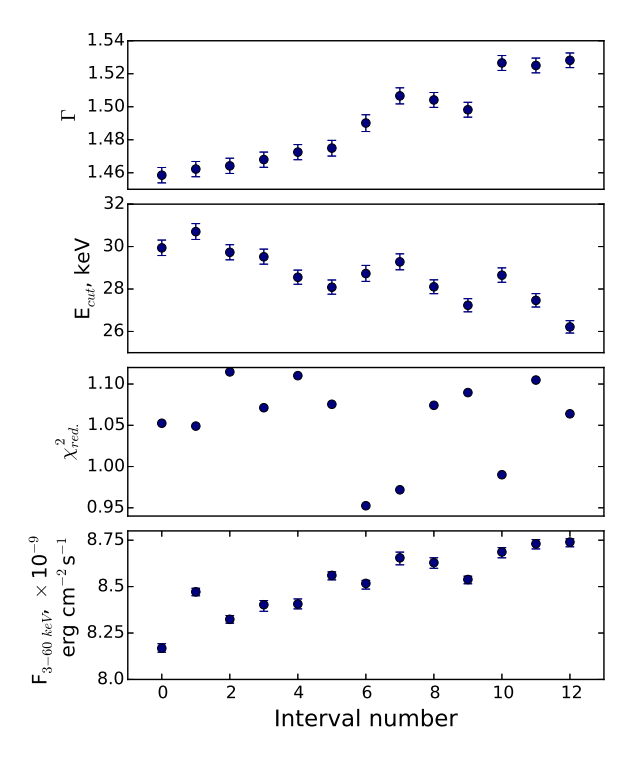

Figure 4. Parameters of continuum emission in intervals. From upper to lower: `xillver` powerlaw slope, cutoff energy, χ^2 per degree of freedom, flux in 3–60 keV band.
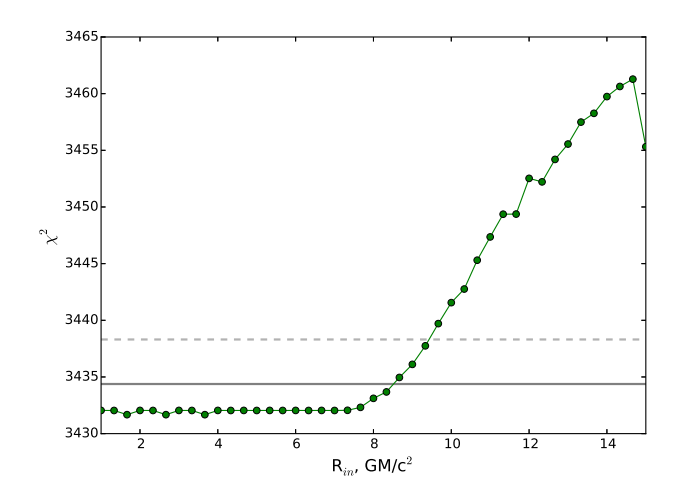
Figure 5. Estimate of inner radius of accretion disk. Gray solid line denote 90% confidence interval, while dashed line shows 99% interval.

Best-fit parameters are presented in

5 TIMING ANALYSIS

Variability properties of different types of X-ray binary systems are usually described in terms of the power spectrum, which is a common technique for determination of amount of power in the particular frequency range. Power spectrum of the BHC systems in LHS typically can be described as a combination of band-limited noise and one or few narrow Lorentzian functions, representing correspondingly broad band stochastic noise and QPOs (see, e.g. Terrell 1972; Belloni and Hasinger 1990; Homan and Belloni 2005b, e.t.c.). Properties of this components and correlations between them, in principle, may be used to discriminate between different models, proposed for generation of X-ray emission in BHC.

Although power spectra analysis is by far the most popular, more sophisticated methods, such as coherence function or phase-lag were successfully used to infer physical properties of accretion flows. Using a measured time-lag between the soft and hard emission, which have a complex behavior with the frequency, Nowak et al. (1999) constrained geometrical size of the accretion flow.

In the following section we present analysis of the timing properties and their evolution during the 2014 outburst of GRS 1739-278 .

5.1 Power spectrum

NuSTAR observation of the GRS 1739-278 2014 outburst are split in 13 continuous intervals separated with ~ 0.7 hr periods when the source was occulted by Earth. The intervals have a duration from ~ 2440 to ~ 3390 sec see Table 1. Since *NuSTAR* detectors operate in the photon counting mode, data can be reduced to the light-curve with time resolution up to 2μs. For our analysis we extracted light-curves with 0.01 s temporal resolution, therefore we obtained power spectra in the $\sim 3 \times 10^{-3}$–50 Hz range. This is a frequency range which usually contains low frequency QPOs

and broad band noise component (Wijnands and van der Klis 1999b). We didn't try to found high frequency QPOs, since the typical HF QPO (centroid frequency 100-400 Hz, amplitude $\approx 10\%$ and quality $Q \approx 0.1$–0.5) is indiscernible over the Poisson noise with the obtained count-rate of ≈ 150 counts per second.

The power spectrum of each of the separate observations has a form of a white noise plateau ($P(f) \propto const$) on the low frequencies, transforming on the frequency ≈ 0.1 Hz in to the power law with the slope $\rho \approx -1.6 - -2.0$. A prominent QPO also present on frequencies 0.3–0.7 Hz along with its second overtone. Poisson noise dominates intrinsic source variability on the frequencies over ≈ 2 Hz, preventing analysis of any high-frequency features. There is also signs that the power spectrum on the frequencies below ≈ 0.003 Hz has a form of growing power law $P(f) \propto f^{\alpha}$, $\alpha > 0$. From the shape of the energy and power spectrum we concluded that the system is in the hard intermediate state and observed low frequency QPO is of type C.

In order to assess properties of the variability power spectra we approximate each obtained power spectra with the following analytical function:

$$
\begin{aligned}
P(f) = n(1 + (f/f_{\text{lb}})^4)^{\alpha} + \\
\frac{s_1}{(f - f_{qpo})^2 + (f_{\text{qpo}}Q_{\text{m}})^2} + \\
\frac{s_2}{(f - 2f_{qpo})^2 + (2f_{\text{qpo}}Q_{\text{m}})^2} + \\
+ poiss
\end{aligned}
\tag{1}
$$

In this function first component represents plateau with the break which can be sharp or smooth, second two components describe QPO fundamental frequency and its first overtone, and a fourth component represents constant Poisson noise.

Due to the complex dead-time behavior over the energy, its impact on to the power spectrum can not be well described. Bachetti et al. (2015) proposed to use real part of the cross-product between two independent *NuSTAR* modules for the power spectrum assessment ($P(f) \approx real(F(f)^*_{\text{fpma}}F(f)_{\text{fpmb}}$, where $F(f)_{\text{FPMA}}$ and $F(f)_{\text{FPMB}}$ - are measured Fourier signal on corresponding frequency f and * - complex conjugation operation) in order to exclude both Poisson noise and dead time effects. This method is based on the following assumption: since photons arrival times are independent for the two detectors, phases of the Fourier function of two light-curves are also random and independent. It follows that this cross-product is a complex value with random uniformly distributed phase and the mean of it's real part is zero. Following Bachetti et al. (2015) we calling obtained function cross-spectrum or cospectrum.

While cross-spectrum technique works perfectly for the power spectrum assessment, we still using classical Fourier power spectrum for the analysis in this work due to the following reason. Each value of the cross-spectrum belongs two the distribution with a complex probability density function (PDF), which, for the random independent signals in two detectors, can be described with the special Bessel function of second kind and has a different PDF for a coherent signals. Since this distribution has finite standard deviation, according to the central limit theorem, distribution of the sum of the values tends toward a normal distribution. To track the source variability evolution we fitting relatively short obser-

Table 1. Evolution of the Fourier and energy spectrum properties through the *NuSTAR* observation in the 3–5 keV energy band.

Interval	T_{start}, MJD	Expo, s	f_{br}, $\times 10^{-2}$, Hz	f_{qpo}, Hz	Q_m, $\times 10^{-2}$	A_m, (rms/mean) %	A_o, (rms/mean) %	rms, %	Γ	E_{cut},
I	56742.68	3386	$9.0^{+2.5}_{-2.5}$	0.30 ± 0.01	$7.2^{+2.5}_{-1.8}$	$7.4^{+1.1}_{-1.2}$	$3.9^{+1.1}_{-1.3}$	27 ± 3	$(145.9 \pm 0.5) \times 10^{-2}$	$29.9 \pm$
II	56742.75	3388	$8.8^{+2.6}_{-2.3}$	0.31 ± 0.01	$8.5^{+2.6}_{-2.2}$	7.6 ± 1.2	$3.3^{+1.1}_{-1.2}$	24^{+3}_{-2}	$(146.2 \pm 0.5) \times 10^{-2}$	$30.7 \pm$
III	56742.81	3392	$9.1^{+3.2}_{-2.3}$	0.34 ± 0.01	$8.7^{+3.3}_{-2.2}$	7.2 ± 1.2	$3.9^{+1.0}_{-1.2}$	26 ± 3	$(146.4 \pm 0.5) \times 10^{-2}$	$29.7 \pm$
IV	56742.88	3389	$8.3^{+2.5}_{-2.1}$	0.35 ± 0.01	$8.6^{+2.4}_{-2.2}$	$7.3^{+1.1}_{-1.2}$	$4.2^{+1.1}_{-1.3}$	27^{+4}_{-3}	$(146.8 \pm 0.5) \times 10^{-2}$	29.5^{+}
V	56742.95	3389	$7.2^{+2.0}_{-1.9}$	0.39 ± 0.01	$8.6^{+2.7}_{-2.1}$	$7.1^{+1.0}_{-1.1}$	$4.4^{+1.2}_{-1.3}$	27^{+4}_{-3}	$(147.3 \pm 0.5) \times 10^{-2}$	$28.6 \pm$
VI	56743.02	3136	$7.2^{+2.1}_{-2.0}$	0.41 ± 0.01	$7.1^{+2.0}_{-1.8}$	7.0 ± 1.1	$4.8^{+1.1}_{-1.2}$	27^{+4}_{-3}	$(147.5 \pm 0.5) \times 10^{-2}$	$28.1 \pm$
VII	56743.09	2771	$8.4^{+2.5}_{-2.2}$	0.42 ± 0.02	$13.0^{+4.0}_{-3.0}$	$7.3^{+1.2}_{-1.2}$	$4.1^{+1.4}_{-1.2}$	25^{+4}_{-3}	1.5 ± 0.0	$28.7 \pm$
VIII	56743.15	3387	$6.0^{+1.8}_{-1.7}$	0.46 ± 0.01	$7.2^{+2.5}_{-1.9}$	$6.6^{+1.1}_{-1.1}$	$3.8^{+1.1}_{-1.3}$	30^{+6}_{-5}	$(150.7 \pm 0.5) \times 10^{-2}$	$29.3 \pm$
IX	56743.22	3392	$13.0^{+3.0}_{-3.0}$	0.49 ± 0.02	$15.0^{+4.0}_{-3.0}$	$9.8^{+0.9}_{-1.1}$	$6.6^{+1.0}_{-1.2}$	21 ± 1	$(150.4 \pm 0.5) \times 10^{-2}$	$28.1 \pm$
X	56743.29	3390	$7.9^{+2.4}_{-2.5}$	0.54 ± 0.01	$7.8^{+2.1}_{-1.8}$	$7.9^{+1.1}_{-1.0}$	$5.3^{+1.2}_{-1.0}$	26^{+5}_{-3}	$(149.8 \pm 0.5) \times 10^{-2}$	$27.2 \pm$
XI	56743.35	3382	$6.3^{+2.3}_{-1.9}$	0.57 ± 0.01	$7.8^{+2.0}_{-1.7}$	8.3 ± 1.0	$4.1^{+1.1}_{-1.4}$	26^{+5}_{-3}	$152.7^{+0.4}_{-0.5} \times 10^{-2}$	$28.7 \pm$
XII	56743.42	3386	$7.1^{+2.4}_{-2.2}$	0.63 ± 0.01	$8.8^{+2.7}_{-1.7}$	$8.9^{+1.0}_{-1.1}$	$5.1^{+1.2}_{-1.3}$	26^{+6}_{-3}	$(152.5 \pm 0.4) \times 10^{-2}$	$27.5 \pm$
XIII	56743.49	3391	$6.8^{+2.2}_{-2.1}$	0.67 ± 0.01	$6.5^{+2.0}_{-1.4}$	$8.8^{+1.0}_{-0.9}$	$4.4^{+1.1}_{-1.2}$	27^{+6}_{-4}	$(152.8 \pm 0.4) \times 10^{-2}$	$26.2 \pm$

vations with duration of 2–3 ks, and therefore can not split them more than to few dozens parts in order to have an eye on the power spectrum break feature on the 0.1 Hz frequency. We found that usual root mean square technique, used to fit normally distributed values, works not stable in that case, probably because the PDF is not yet close enough to the normal distribution.

To simplify our analysis we inspect power spectrum only on frequencies below 10 Hz, allowing Poisson noise to have arbitrary power but assuming that its power spectrum component is still flat ($P(f) = const$).

We found that the QPO frequency and amplitude clearly evolves with time see Table 1 and Figure 7. The QPO frequency correlates with the *NuSTAR* flux and photon index, similar to many other black hole and neutron star binary systems (see, e.g., Vignarca et al. 2003; Pottschmidt et al. 2003). On the other hand we see, that the QPO amplitude was stable during the first half of the observation, and started to grow up in the second part.

Some models suggest, that the type-C QPO arise due to the Lense-Thirring precession of the inner parts of the accretion flow (Stella and Vietri 1998b; Schnittman et al. 2006; Ingram et al. 2009b), in such models growth of the QPO frequency corresponds to the shrinking of the disk inner radius (so called *truncation* radius). However, sophisticated spectral models applied to the observed *NuSTAR* spectrum suggest that the accretion disk inner radius is $R_{in} = 5^{+4}_{-3} R_g$. This estimation is primarily based on the profile of the relativistically broadened neutral iron fluorescent line, see section **??** and also (Miller et al. 2015).

We found that the QPO amplitude is smaller in the soft band, while amplitude of it's harmonic is bigger, the ratio of the power in the QPO and it's harmonic is 0.2 ± 0.1 in 10–78 keV band and 0.4 ± 0.1 in 3-5 energy band. It follows that the QPO profile, if it is presented (see, e.g. Ingram and van der Klis 2015), differs in the hard and soft X-ray band. Following (Ingram and van der Klis 2015) we tried to extract QPO profile segregating the coherent part between the QPO and it's harmonic, however no significant coherence was presented above the noise level, one can conclude that the QPO profile was not stable.
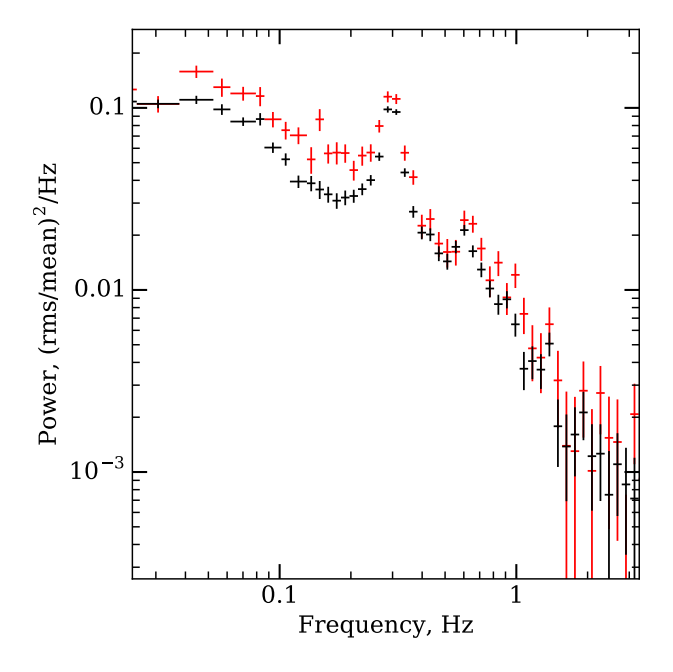

Figure 6. Cross-spectrum of the observations, obtained by scaling frequency to conserve QPO position. Black crosses obtained from the all data sets, while red crosses are from sets I, II, IV, and V, in which QPO subharmonics was most prominent.

In some observation segments QPO subharmonics, centered approximately at the 1/2 of the QPO centroid frequency, is clearly observed in the cross-spectra (see examples on Figure **??**, red crosses) (namely I, II, IV, V, VI sets). In order to observe QPO profile with better significance we summarized several cospectra, frequency of each cospectrum was scaled such a way to conserve QPO centroid at 0.3 Hz. Obtained tracked cospectrum is presented on Figure 6.

The subharmonics seems to roam around the 1/2 QPO frequency, therefore we were not able to obtain it with a large significance on the tracked spectrum.

It should be noted that the changes in the QPO centroid position may contribute in the observed quality fac-

tor Q. We can estimate the derivative of the QPO centroid position with time (by approximating $f_{\mathrm{QPO}}(time)$ with the straight line), which appears to be $\dot{f}_{\mathrm{QPO}} \approx 6.5 \times 10^{-6}$ Hz s^{-1}. During an observation with the duration $\tau = 3000$ s even perfect QPO located at $f_{\mathrm{QPO}} = 0.3$ Hz is observed with the quality factor $Q \approx \dot{f}_{\mathrm{QPO}}\tau/f_{\mathrm{QPO}} \approx 0.065$, which is of order of the Q estimations obtained from the observations with 1 model. In order to better estimate the QPO quality factor, we separated each of the 13 observations on 82 s time-series. Power spectra in each observation we fitted simultaneously substituting in the model 1 instead of the QPO centroid frequency $f_{\mathrm{qpo}} + (t - t_{\mathrm{mid}})\dot{f}_{\mathrm{qpo}}$, with $\dot{f}_{\mathrm{qpo}}$ being the free parameter, f_{qpo} QPO centroid position estimated for the model1 and t_{mid} middle of the data set observation time interval. Inside each data set we obtained the QPO centroid changing speed consistent with the estimation obtained from the general trend, nevertheless the median quality factor, obtained in this model appears to be $\sim 7 \times 10^{-2}$ - i.e. compatible with the previous estimations (see Table 1).

In Table **??** one can fined obtained fit parameters for the 13 separate uninterrupted *NuSTAR* time series.

5.2 Coherence

Power spectra of XBs are often have a complex shape with broad band noise and QPO like features, and numerous different models of these system were suggested to explain each particular feature. (**?**) suggested to use coherence between different energy bands in order to obtain additional information on the source time properties. They define coherence as

$$C(f) = \frac{|<H(f)^* S(f)>|^2}{<|H(f)|^2><|S(f)|^2>} \qquad (2)$$

where $H(f)$ and $S(f)$ are Fourier function of time series in hard and soft bands correspondingly. This function demonstrates the similarity of stochastic time signal in both bands. Different models of the XBs variability formation suggest that the signal in two energy bands can be partially independent, while the shape of the power spectra is conserved. It appears that in many sources coherence between soft and hard X-ray bands is close to unity (**???**), in contrary to different models predictions (see, discussion in **?**).

Following method (**?**) we estimated correlation of GRS 1739-278 light-curves obtained in the soft and hard energy bands. Since for the timing analysis we use *NuSTAR* data, we adopt following energy bands for the soft and hard light-curves correspondingly: 3–10 keV (soft) and 10–79 keV (hard).

In contrast to the (**?**) study, net count rate, obtained in GRS 1739-278 *NuSTAR* observation is **160 s^{-1}**, it follows that approximately quarter of the total variability power is due to the Poisson noise. As was discussed in (**?**) the correlation of two independent time series demonstrates large errors on the frequencies dominated with Poisson noise, due to the random walk in the 2-D complex space. We also found, that the correlation of the light-curves obtained from *NuSTAR* is subjected by the dead-time and crosstalk effects between the energy bands. In order to eliminate this effects, following the recipe suggested in Bachetti et al. (2015) for power spectra estimation, we find crossproducts of the light-curves Fourier functions obtained on the different modules - e.g.

correlations of the light-curve obtained in the soft band on the FPMA module with the light-curve in the hard band obtained in the FPMB and vice versa. Obtained correlation does not contain polluting signal from the blocking dead time.

After that, as explained in (**?**), one should find the amplitude of the fully coherent signal $<|H(f)|^2><|S(f)|^2>$ in order to estimate coherence of the signals. There is several different options, which one can be use to estimate this normalization:

(i) Use observed of the power spectra in each energy band. The drawback of this method is that power spectra contain Poisson noise component constant on all frequencies and dominating over the source variability on high frequencies. Thus, since Poisson noise is not coherent, if one use this normalization as a denominator in Eq. 2 coherence estimation will be dumped on the value equal to the ratio of the Poisson noise to the source signal power on each frequency.

(ii) Instead of the observed power spectra, one can use approximation of the power spectra with analytical models. Poisson noise component can be discarded in analytical model, thus only source signal is conserved. The drawback is that due to the Dead time effects Poisson noise has a complex form and can not be easily estimated with simple model.

(iii) Use coherent part of the Fourier function of light curves in two modules (Bachetti et al. 2015) or it's approximation with the analytical function. It should be noted, that obtained coherent part of the $\mathrm{re}(H_A(f)^* H_B(f))$ has complex statistic which not restricting negative values, which must be ignored or modified thus affecting result. We also found, that for short time series, one should use more complex likelihood criterion in order to fit coherent signal with analytical functions, since the statistic is still far from Gaussian and obtained fits are often unstable.

On Figure 8 presented measured coherence between hard and soft bands on the frequencies up to ~ 1 Hz. Two methods were used to obtain coherence, first we use cross spectra as an assessmnet to the signals variability power in each band (black crosses on Figure 8, and second we used analytical models obtained via fitting direct power spectra and subtracting Poisson noise component (red crosses). The data after that was rebinned it to the logarithmical bins and the error were estimated statisticaly as a standard deviation of values in each bins. Coherence in the first few frequency channels were not binned, instead, observations were split on several subsets, coherence in this subsets were obtained and standard deviation of that samples were estimated. Since we have only 13 separate observations, standard deviation was obtained with very few degrees of freedom and therefore is underestimated.

We found that, while coherence is of order of unity in the close energy bands (3–5 to 5–8 keV and 8–15 to 15–78 keV) it drops down to ≈ 0.8 between hard and soft bands (3–5 to 15–78 keV) which is not similar to results obtained for Cyg X-1 (**?**). It worth nothing, that the energy spectrum obtained with *NuSTAR* can be explained with two absorbed spectral components (powerlaw plus relativisticly broadened fluorescent Fe Kα line), see Sec. **??**. There is no clear changes in the coherence on the QPO frequency, i.e. soft and energy bands is not fully coherent.
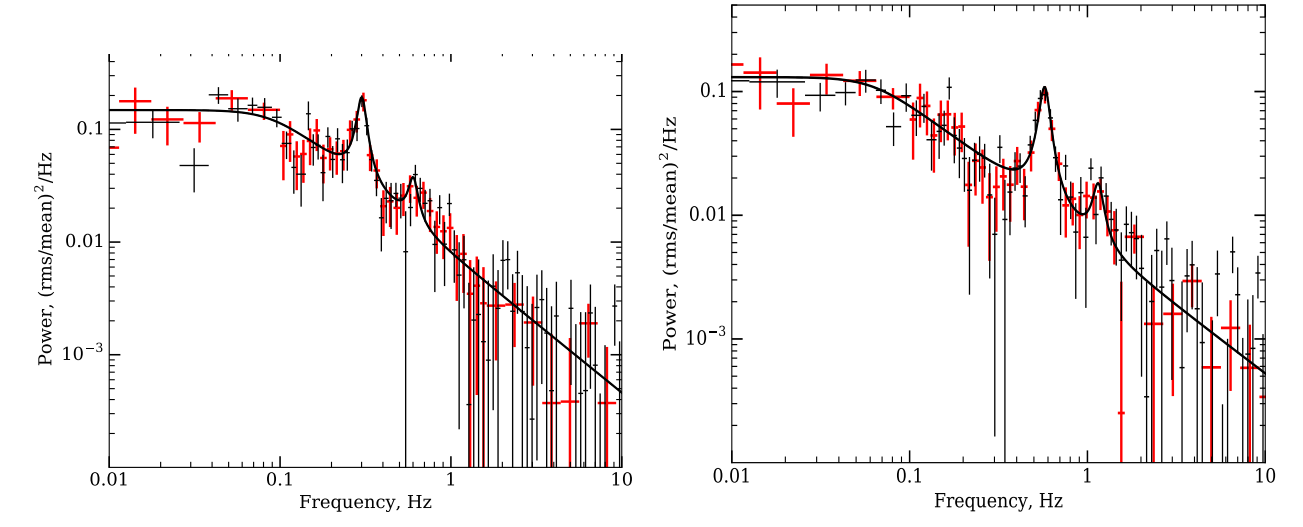
Figure 7. On the left panel power spectrum and cospectrum obtained in the soft band at the beginning of *NuSTAR* observation. On the right column same spectra obtained at the end of the observation. Red crosses correspond to the power spectrum with Poisson noise component subtracted, and black crosses correspond to cospectrum. Black line represents best model for the power spectrum without Poisson noise component.
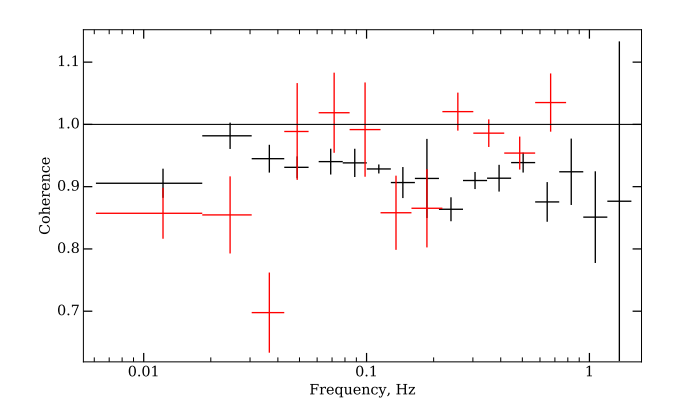

Figure 8. Coherence between the soft (3–10 keV) and hard (10–78 keV) energy bands as a function of frequency. Black crosses represent estimations made with the both cross components and power spectra are obtained from data. Red crosses obtained from the cross component obtained from divided by the power spectra analytical models with Poisson noise components subtracted.

5.3 Phase lags

Following ([Vaughan and Nowak 1997](#)) we estimate phase lag as an angle of mean product of the light curves Fourier harmonics from one energy bands to the conjugated Fourier harmonics of second energy band.

$$P_{\text{hs}} = F_h(f)^* F_s(f) \tag{3}$$

We can imagine that each light curve from a sample consist of stochastic noise and coherent signal $F_{\text{h[s]}} = n e^{-i\alpha}$, where i - is complex unit, k - amplitude of the Fourier harmonic and α its phase. Amplitudes of each harmonic in that case are distributed with the Normal distribution with zero mean, and divergence equal to the square power in particular frequency band. The probability density function (PDF) of the product of two Normal distribution described with

the modified Bessel function of second kind with 0-th order. Result of the product of two Foruier harmonics can be represented ad a sum of four complex numbers, amplitude of each is distributed with PDF having a form of modified Bessel function, phases of three of these numbers distributed uniformly, and phase of the last one is distributed nonuniformly with mean equal to real phase shift between two coherent signals. We can now determine the "phase axis" as the axis along the mean complex value of the Sample. Distribution of the points relative to the "phase axis" obviously should be symmetrical, and along it should be assymetric and shifted towards the mean complex value of the sample. If we now rotate all the obtained complex Fourier harmonics in our sample along this axis $\frac{<P_{\text{hs}}^*>P_{\text{hs}}}{|<P_{\text{hs}}>|}$, real part of each value is the projection on the "phase axis" and imaginary part is projection on the perpendicular axis. We found that the distribution of the projected on the "phase axis" values is closely resembles assymetric Laplace distribution and the distribution of the points projected on the perpendicular axis resembles symmetric Laplace distribution. Bearing this in mind we estimate mean value for each of the four distributions (positive real, negative real, positive imaginary and negative imaginary) and assess variances of this distribution. Since we accepted that each of these distribution has a PDF close to exponential we take their variance as a variance of χ_2^{2N} distribution, where N - is a number of entities in the each sample. After that we accept the error on the phase to be equal π if the mean of positive real sample is less than the square root of the sum of the positive and negative real samples variances, otherwise we take it to be equal

$$\Delta\phi = atan\left(\frac{\sqrt{v_{i-}^2 + v_{i+}^2}}{m_{r+} - m_{r-} - \sqrt{v_{r+}^2 + v_{r-}^2}}\right) \tag{4}$$

Error assessment for the phase lag points position

Most of the models of the accretion flow which describe variability and energy spectra formation, suggest the time
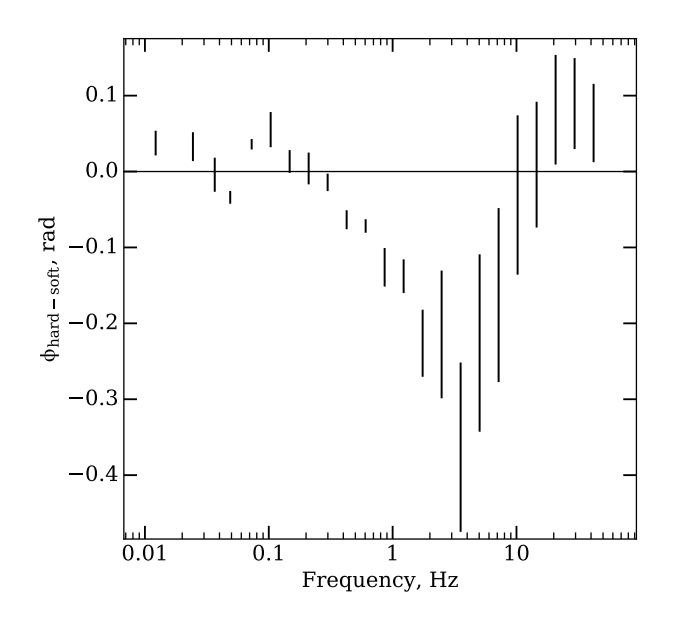
Figure 9. Phase lag between the hard (10–78 keV) and soft (3–10) energy bands in GRS 1739-278

5.4 timinig discussion

We found that the total power in the second QPO harmonic in the soft band is comparable to the total power in the main harmonic, in the hard band second harmonic is ≈ 3 times less powerfull than the main. Total power of the harmonics growing with the source count-rate and QPO frequency in the soft and hard energy bands (see Table 1).

REFERENCES

Arévalo, P. and Uttley, P.: 2006, *MNRAS* **367**, 801

Arnaud, K. A.: 1996, in G. H. Jacoby and J. Barnes (eds.), *Astronomical Data Analysis Software and Systems V*, Vol. 101 of *Astronomical Society of the Pacific Conference Series*, p. 17

Bachetti, M., Harrison, F. A., Cook, R., Tomsick, J., Schmid, C., Grefenstette, B. W., Barret, D., Boggs, S. E., Christensen, F. E., Craig, W. W., Fabian, A. C., Fürst, F., Gandhi, P., Hailey, C. J., Kara, E., Maccarone, T. J., Miller, J. M., Pottschmidt, K., Stern, D., Uttley, P., Walton, D. J., Wilms, J., and Zhang, W. W.: 2015, *ApJ* **800**, 109

Belloni, T. and Hasinger, G.: 1990, *A&A* **227**, L33

Belloni, T. M.: 2010, in T. Belloni (ed.), *Lecture Notes in Physics, Berlin Springer Verlag*, Vol. 794 of *Lecture Notes in Physics, Berlin Springer Verlag*, p. 53

Borozdin, K. N., Revnivtsev, M. G., Trudolyubov, S. P., Aleksandrovich, N. L., Sunyaev, R. A., and Skinner, G. K.: 1998, *Astronomy Letters* **24**, 435

Borozdin, K. N. and Trudolyubov, S. P.: 2000, *ApJ* **533**, L131

Cabanac, C., Henri, G., Petrucci, P.-O., Malzac, J., Ferreira, J., and Belloni, T. M.: 2010, *MNRAS* **404**, 738

Casella, P., Belloni, T., and Stella, L.: 2005, *ApJ* **629**, 403

Churazov, E., Gilfanov, M., and Revnivtsev, M.: 2001, *MNRAS* **321**, 759

Dauser, T., García, J., Parker, M. L., Fabian, A. C., and Wilms, J.: 2014, *MNRAS* **444**, L100

Dauser, T., García, J., Walton, D. J., Eikmann, W., Kallman, T., McClintock, J., and Wilms, J.: 2016, *A&A* **590**, A76

Eardley, D. M., Lightman, A. P., and Shapiro, S. L.: 1975, *ApJ* **199**, L153

Evans, P. A., Beardmore, A. P., Page, K. L., Osborne, J. P., O'Brien, P. T., Willingale, R., Starling, R. L. C., Burrows, D. N., Godet, O., Vetere, L., Racusin, J., Goad, M. R., Wiersema, K., Angelini, L., Capalbi, M., Chincarini, G., Gehrels, N., Kennea, J. A., Margutti, R., Morris, D. C., Mountford, C. J., Pagani, C., Perri, M., Romano, P., and Tanvir, N.: 2009, *MNRAS* **397**, 1177

Filippova, E., Kuulkers, E., Skådt, N. M., Alfonso-Garzon, J., Beckmann, V., Bird, A. J., Brandt, S., Chenevez, J., Del Santo, M., Domingo, A., Ebisawa, K., Jonker, P. G., Kretschmar, P., Markwardt, C. B., Oosterbroek, T., Paizis, A., Pottschmidt, K., Sanchez-Fernandez, C., Wijnands, R., Bozzo, E., and Ferrigno, C.: 2014, *The Astronomer's Telegram* 5991

Fuerst, F., Tomsick, J. A., Yamaoka, K., Dauser, T., Miller, J. M., Clavel, M., Corbel, S., Fabian, A. C., Garcia, J., Harrison, F. A., Loh, A., Kaaret, P., Kalemci, E., Migliari, S., Miller-Jones, J. C. A., Pottschmidt, K., Rahoui, F., Rodriguez, J., Stern, D., Stuhlinger, M., Walton, D. J., and Wilms, J.: 2016, *ArXiv e-prints*

García, J., Dauser, T., Reynolds, C. S., Kallman, T. R., McClintock, J. E., Wilms, J., and Eikmann, W.: 2013, *ApJ* **768**, 146

Grebenev, S. A., Sunyaev, R. A., and Pavlinsky, M. N.: 1997, *Advances in Space Research* **19**, 15

lag between the signals in different energy bands. For example in some models of the energy spectra formation, time lag is naturally arise due to the geometry of the corona and properties of the inverse Comptonization process (see, e.g. **?**). Phase lag is also suggested from the propagating fluctuations model - hard photons are emitted from the inner parts of the accretion flow from the perturbations, which initially were born in the outer parts of the disk were produce soft emission.

It also was found, that phase lag of XBs, probably depends on the system inclination angle (**?**), it also definitely contain information about the characteristic times of the system, and therefore can be proxy to the compact object mass ().

Phase lags can be estimated as a product of the mean phase of the set of Fourier spectra and the corresponding frequency:

$$\tau = \frac{\phi(f)}{2\pi f} \qquad (5)$$

$$\phi(f) = < arccos\left(\frac{re(< F_{\mathrm{h}}^*(f)F_{\mathrm{s}}(f) >)}{|F_{\mathrm{h}}^*(f)F_{\mathrm{s}}(f)|}\right) > \qquad (6)$$

here, $F_h(f)$ and $F_s(f)$ are Fourier functions of the lightcurves in the hard and soft bands, $\phi(f)$ is the phase lag.

We found that phase lag on each frequency is generally conserved along the observation. In order to improve significance we compute phase lag for all 13 time series. Obtained phase lag for frequencies from 10^{-2} Hz to 100 Hz is presented in Figure 9. As follows from the Eq. 6 we compute phase shift between the phases of the Fourier harmonics in hard and soft lightcurves, therefore negative phase lag corresponds to the hard lag. It Follows from Figure 9 that there is soft lag on low frequencies which transforms in to the hard lag on frequencies grater than QPO frequency.

Greiner, J., Dennerl, K., and Predehl, P.: 1996, *A&A* **314**, L21

Harrison, F. A., Craig, W. W., Christensen, F. E., Hailey, C. J., Zhang, W. W., Boggs, S. E., Stern, D., Cook, W. R., Forster, K., Giommi, P., Grefenstette, B. W., Kim, Y., Kitaguchi, T., Koglin, J. E., Madsen, K. K., Mao, P. H., Miyasaka, H., Mori, K., Perri, M., Pivovaroff, M. J., Puccetti, S., Rana, V. R., Westergaard, N. J., Willis, J., Zoglauer, A., An, H., Bachetti, M., Barrière, N. M., Bellm, E. C., Bhalerao, V., Brejnholt, N. F., Fuerst, F., Liebe, C. C., Markwardt, C. B., Nynka, M., Vogel, J. K., Walton, D. J., Wik, D. R., Alexander, D. M., Cominsky, L. R., Hornschemeier, A. E., Hornstrup, A., Kaspi, V. M., Madejski, G. M., Matt, G., Molendi, S., Smith, D. M., Tomsick, J. A., Ajello, M., Ballantyne, D. R., Baloković, M., Barret, D., Bauer, F. E., Blandford, R. D., Brandt, W. N., Brenneman, L. W., Chiang, J., Chakrabarty, D., Chenevez, J., Comastri, A., Dufour, F., Elvis, M., Fabian, A. C., Farrah, D., Fryer, C. L., Gotthelf, E. V., Grindlay, J. E., Helfand, D. J., Krivonos, R., Meier, D. L., Miller, J. M., Natalucci, L., Ogle, P., Ofek, E. O., Ptak, A., Reynolds, S. P., Rigby, J. R., Tagliaferri, G., Thorsett, S. E., Treister, E., and Urry, C. M.: 2013, *ApJ* **770**, 103

Heil, L. M., Uttley, P., and Klein-Wolt, M.: 2015, *MNRAS* **448**, 3339

Hjellming, R. M., Rupen, M. P., Marti, J., Mirabel, F., and Rodriguez, L. F.: 1996, *IAU Circ.* 6383

Homan, J. and Belloni, T.: 2005a, *Ap&SS* **300**, 107

Homan, J. and Belloni, T.: 2005b, *Ap&SS* **300**, 107

Ingram, A., Done, C., and Fragile, P. C.: 2009a, *MNRAS* **397**, L101

Ingram, A., Done, C., and Fragile, P. C.: 2009b, *MNRAS* **397**, L101

Ingram, A. and van der Klis, M.: 2013, *MNRAS* **434**, 1476

Ingram, A. and van der Klis, M.: 2015, *MNRAS* **446**, 3516

Ingram, A., van der Klis, M., Middleton, M., Done, C., Altamirano, D., Heil, L., Uttley, P., and Axelsson, M.: 2016, *MNRAS* **461**, 1967

Krimm, H. A., Barthelmy, S. D., Baumgartner, W., Cummings, J., Gehrels, N., Lien, A. Y., Markwardt, C. B., Palmer, D., Sakamoto, T., Stamatikos, M., and Ukwatta, T.: 2014, *The Astronomer's Telegram* 5986

Krimm, H. A., Holland, S. T., Corbet, R. H. D., Pearlman, A. B., Romano, P., Kennea, J. A., Bloom, J. S., Barthelmy, S. D., Baumgartner, W. H., Cummings, J. R., Gehrels, N., Lien, A. Y., Markwardt, C. B., Palmer, D. M., Sakamoto, T., Stamatikos, M., and Ukwatta, T. N.: 2013, *ApJS* **209**, 14

Lyubarskii, Y. E.: 1997, *MNRAS* **292**, 679

Marti, J., Mirabel, I. F., Duc, P.-A., and Rodriguez, L. F.: 1997, *A&A* **323**, 158

Matsuoka, M., Kawasaki, K., Ueno, S., Tomida, H., Kohama, M., Suzuki, M., Adachi, Y., Ishikawa, M., Mihara, T., Sugizaki, M., Isobe, N., Nakagawa, Y., Tsunemi, H., Miyata, E., Kawai, N., Kataoka, J., Morii, M., Yoshida, A., Negoro, H., Nakajima, M., Ueda, Y., Chujo, H., Yamaoka, K., Yamazaki, O., Nakahira, S., You, T., Ishiwata, R., Miyoshi, S., Eguchi, S., Hiroi, K., Katayama, H., and Ebisawa, K.: 2009, *PASJ* **61**, 999

Mereminskiy, I., Krivonos, R., Grebenev, S., Filippova, E., and Sunyaev, R.: 2016, *The Astronomer's Telegram* 9517

Miller, J. M., Homan, J., and Miniutti, G.: 2006a, *ApJ* **652**, L113

Miller, J. M., Homan, J., Steeghs, D., Rupen, M., Hunstead, R. W., Wijnands, R., Charles, P. A., and Fabian, A. C.: 2006b, *ApJ* **653**, 525

Miller, J. M., Tomsick, J. A., Bachetti, M., Wilkins, D., Boggs, S. E., Christensen, F. E., Craig, W. W., Fabian, A. C., Grefenstette, B. W., Hailey, C. J., Harrison, F. A., Kara, E., King, A. L., Stern, D. K., and Zhang, W. W.: 2015, *ApJ* **799**, L6

Molteni, D., Sponholz, H., and Chakrabarti, S. K.: 1996, *ApJ* **457**, 805

Narayan, R. and Yi, I.: 1995, *ApJ* **452**, 710

Nowak, M. A., Wilms, J., and Dove, J. B.: 1999, *ApJ* **517**, 355

Parker, M. L., Tomsick, J. A., Miller, J. M., Yamaoka, K., Lohfink, A., Nowak, M., Fabian, A. C., Alston, W. N., Boggs, S. E., Christensen, F. E., Craig, W. W., Fürst, F., Gandhi, P., Grefenstette, B. W., Grinberg, V., Hailey, C. J., Harrison, F. A., Kara, E., King, A. L., Stern, D., Walton, D. J., Wilms, J., and Zhang, W. W.: 2015, *ApJ* **808**, 9

Paul, J., Bouchet, L., Churazov, E., and Sunyaev, R.: 1996, *IAU Circ.* 6348

Paul, J., Mandrou, P., Ballet, J., Cantin, M., Chabaud, J., Cordier, B., Ehanno, M., Goldwurm, A., Lambert, A., Lande, J., et al.: 1991, *Advances in Space Research* **11(8)**, 289

Pottschmidt, K., Wilms, J., Nowak, M. A., Pooley, G. G., Gleissner, T., Heindl, W. A., Smith, D. M., Remillard, R., and Staubert, R.: 2003, *A&A* **407**, 1039

Remillard, R. A. and McClintock, J. E.: 2006, *ARA&A* **44**, 49

Ross, R. R. and Fabian, A. C.: 2005, *MNRAS* **358**, 211

Schnittman, J. D., Homan, J., and Miller, J. M.: 2006, *ApJ* **642**, 420

Shakura, N. I. and Sunyaev, R. A.: 1973, *A&A* **24**, 337

Shapiro, S. L., Lightman, A. P., and Eardley, D. M.: 1976, *ApJ* **204**, 187

Stella, L. and Vietri, M.: 1998a, *ApJ* **492**, L59

Stella, L. and Vietri, M.: 1998b, *ApJ* **492**, L59

Tagger, M. and Pellat, R.: 1999, *A&A* **349**, 1003

Tanaka, Y. and Shibazaki, N.: 1996, *ARA&A* **34**, 607

Terrell, Jr., N. J.: 1972, *ApJ* **174**, L35

García, J., Dauser, T., Lohfink, A., Kallman, T. R., Steiner, J. F., McClintock, J. E., Brenneman, L., Wilms, J., Eikmann, W., Reynolds, C. S., and Tombesi, F.: 2014, *ApJ* **782**, 76

Vaughan, B. A. and Nowak, M. A.: 1997, *ApJ* **474**, L43

Verner, D. A., Ferland, G. J., Korista, K. T., and Yakovlev, D. G.: 1996, *ApJ* **465**, 487

Vignarca, F., Migliari, S., Belloni, T., Psaltis, D., and van der Klis, M.: 2003, *A&A* **397**, 729

Wijnands, R. and van der Klis, M.: 1999a, *ApJ* **514**, 939

Wijnands, R. and van der Klis, M.: 1999b, *ApJ* **514**, 939

Wilms, J., Allen, A., and McCray, R.: 2000, *ApJ* **542**, 914

Yan, Z. and Yu, W.: 2017, *Monthly Notices of the Royal Astronomical Society* **470(4)**, 4298

This paper has been typeset from a TEX/LATEX file prepared by the author.